Reflective and Fluorescent Separation under Narrow-Band Illumination

Koji Koyamatsu   Daichi Hidaka   Takahiro Okabe
Kyushu Institute of Technology
okabe@ai.kyutech.ac.jp

Hendrik P. A. Lensch
University of Tübingen
hendrik.lensch@uni-tuebingen.de

Abstract

In this paper, we address the separation of reflective and fluorescent components in RGB images taken under narrow-band light sources such as LEDs. First, we show that the fluorescent color per pixel can be estimated from at least two images under different light source colors, because the observed color at a surface point is represented by a convex combination of the light source color and the illumination-invariant fluorescent color. Second, we propose a method for robustly estimating the fluorescent color via MAP estimation by taking the prior knowledge with respect to fluorescent colors into consideration. We conducted a number of experiments by using both synthetic and real images, and confirmed that our proposed method works better than the closely related state-of-the-art method and enables us to separate reflective and fluorescent components even from a single image. Furthermore, we demonstrate that our method is effective for applications such as image-based material editing and relighting.

1. Introduction

Fluorescence is a very common phenomenon observed both in natural objects such as minerals and plants and in man-made objects such as papers and clothes [2]. Fluorescent materials emit light with longer wavelengths than those of the absorbed light, in contrast to reflective materials which reflect light with the same wavelengths as those of the incident light. Separating reflective and fluorescent components in images is important for preprocessing of various computer vision techniques that assume reflective components such as diffuse and specular ones.

Recently, due to the progress of light-emitting diodes (LEDs), narrow-band light sources are often used for illuminating an object of interest and capturing its images in the fields of computer vision and computer graphics [21, 1, 8, 17, 15, 16]. The application domain of images taken under narrow-band light sources includes image-based spectral relighting [21, 16], raw material classification [8], bidirectional texture function (BTF) classification [17], and sur-

face normal and reflectance recovery [15]. Therefore, separating reflective and fluorescent components under narrow-band illumination is useful for preprocessing of such applications.

In this paper, we address the separation of reflective and fluorescent components in RGB images taken under narrow-band light sources such as LEDs. First, we show that the fluorescent color is on the plane spanned by the light source color and the observed pixel color in the RGB color space, and then the fluorescent color per pixel can be estimated from at least two images under different light source colors as the intersection of the two planes. This is because the pixel color is represented by a convex combination of the light source color and the illumination-invariant fluorescent color. Second, we take the prior knowledge with respect to fluorescent colors, *i.e.* the distribution of fluorescent colors in the r-g chromaticity space into consideration, and propose a method for robustly estimating the fluorescent color via maximum a posteriori (MAP) estimation.

Through a number of experiments by using both synthetic and real images, we confirm that our proposed approach works better than the closely related state-of-the-art method [26] based on independent component analysis (ICA) [12]. In addition, we show that our method taking account of the prior knowledge with respect to fluorescent colors enables us to separate reflective and fluorescent components even from a single image. Furthermore, we demonstrate that our method is effective for applications such as image-based material editing and relighting.

The main contribution of this study is threefold. First, we explore the novel problem of separating reflective and florescent components under narrow-band illumination, and show that the fluorescent color per pixel can be estimated from at least two images. Second, we achieve the reflective and fluorescent separation from a single image by taking the known space of potential fluorescent colors into consideration. Third, we show that our approach with the improved model results in better fluorescent separation than closely related state-of-the-art methods, *e.g.* ICA-based method [26], and is effective for applications such as image-based material editing and relighting.

The rest of this paper is organized as follows. In Section 2, we briefly summarize related work. In Section 3, we show that the fluorescent color per pixel can be estimated from at least two images, and then propose a method for reflective-fluorescent separation via MAP estimation. We report the experimental results and the applications in Section 4. We present concluding remarks in Section 5.

2. Related Work

2.1. Properties of fluorescence

The spectral property of a fluorescent surface is described in a bispectral manner by using the *Donaldson matrix* [3]. Each element of the Donaldson matrix is the amount of reflected/emitted light when the wavelengths of the outgoing light (row) and the incoming light (column) are given. The diagonal elements, where the outgoing wavelength is the same as the incoming wavelength, are reflective components, and the lower-left elements, where the outgoing wavelength is longer than the incoming wavelength, are fluorescent components. The spectral property of fluorescent components, *i.e.* a pure fluorescent material without reflective components, is often described more simply by using the *absorption spectrum* and the *emission spectrum* [13]. The former is the fraction of incoming light absorbed by the material, and the latter is the amount of outgoing light emitted from the material at each wavelength.

The amount of reflected/emitted light from a fluorescent surface depends not only on the wavelengths but also on the directions of the incoming light and the outgoing light. In the graphics community, Glassner [7] and Wilkie *et al*. [25] model the angular property of fluorescent components in the same manner as the Lambert model, *i.e.* the fluorescent radiance is proportional to the irradiance. In general, the angular property of a fluorescent surface including reflective components is described by a bispectral bidirectional reflectance and reradiation distribution function (bispectral BRRDF). Hullin *et al*. [11] propose an image-based method for acquiring the bispectral BRRDFs of fluorescent surfaces by extending the image-based method for BRDF acquisition [18] to bispectal measurement. They report that the fluorescent components have weak angular dependency.

One of the interesting behaviors of fluorescence is *wavelength shift* called the Stokes shift; a fluorescent material absorbs incident light at a certain wavelength, and then emits light at longer wavelengths than the incident one. Hullin *et al*. [10] exploit the fact that multiple scattering is suppressed in a fluorescent liquid due to the Stokes shift, and then propose immersion range scanning for shape recovery of transparent objects. Sato *et al*. [23] and Treibitz *et al*. [24] show that fluorescent components approximately obeys the Lambert model with respect to light source directions, and then propose bispectral photometric stereo

based on fluorescence; an object of interest is illuminated by shorter-wavelength light sources and is observed by a longer-wavelength camera band. They show that the bispectral photometric stereo is robust against specular reflection components and interreflections due to the Stokes shift.

Another interesting behavior of fluorescence is *illumination invariance* of fluorescent colors, *i.e* the chromaticity of fluorescent components observed on a fluorescent surface is constant independent of the spectral intensity of incident light. This is because the fluorescent color depends only on the emission spectra and is independent of the absorption spectra. Han *et al*. [9] makes use of the illumination invariance for calibrating the spectral sensitivity of a camera under unknown illumination. The illumination invariance is used also for reflective and fluorescent separation as described in the next subsection.

2.2. Reflective and fluorescent separation

Zhang and Sato [26] propose a method for separating reflective and fluorescent components under the assumption that the spectral sensitivity of a camera is narrow-band as is often assumed in color constancy algorithms. Specifically, their method is based on the *channel-wise* linear model; grayscale images in each channel under varying spectral intensities are represented by convex combinations of a reflective grayscale image and a fluorescent grayscale image. Then, those basis images are computed by using ICA in the high-dimensional image space in a similar manner to reflection removal [4]. Unfortunately, however, such channel-wise linearity does not hold for images taken under narrow-band illumination[1], and then we cannot use their method when not the cameras but the light sources are narrow-band. In this study, we show that our *pixel-wise* linear model can be used for narrow-band illumination instead.

Fu *et al*. [6] propose a method for separating reflective and fluorescent components by using high-frequency illumination in the spectral domain on the basis that the absorption spectra are usually low-frequency. Their method is analogous to the direct-global separation by using high-frequency illumination in the spatial domain [20]. Unfortunately, however, their method requires special and expensive devices: a hyperspectral camera and a programmable illumination in the spectral domain. On the other hand, our proposed method uses a usual color camera and LEDs. In addition, Fu *et al*. [5] propose a method for estimating the spectral properties of reflectance and fluorescence from several RGB images taken under varying spectral intensities. They make use of low-dimensional linear model of spectral reflectance [22] and absorption spectrum, and es-

---

[1]Specifically, N grayscale images in each channel under N narrow-band light sources are represented by the convex combinations of $(N+1)$ basis images, *i.e.* N for reflectance and one for fluorescence in general. Therefore, ICA-based method is ill-posed under narrow-band illumination.

timate their coefficients of the linear combinations. Their method is also related to ours in the sense that the reflective and fluorescent components can be recovered from the basis functions and the estimated coefficients. Unfortunately, however, their method requires 9 images taken under different spectral intensities, and thus the separation from a single image is impossible.

3. Proposed Method

In this section, we explore the reflective and fluorescent model under narrow-band illumination, and derive the intersection method for reflective-fluorescent separation. Furthermore, we exploit the typical color distribution for fluorescent materials [19], and then extend it via MAP estimation.

3.1. Reflective and fluorescent model

We assume that an object of interest is observed by using a color camera. For reflective and fluorescent surfaces, the pixel value $i = (i_R, i_G, i_B)^\top$ at a point on the object surface consists of a reflective component $r = (r_R, r_G, r_B)^\top$ and a fluorescent component $f = (f_R, f_G, f_B)^\top$ in general:

$$i = r + f. \qquad (1)$$

According to the dichromatic reflection model, the reflective component is described by the sum of a diffuse reflection component and a specular reflection component as

$$r_c = g_d \int l(\lambda')\rho(\lambda')s_c(\lambda')d\lambda' + g_s \int l(\lambda')s_c(\lambda')d\lambda'. \qquad (2)$$

Here, λ', $l(\lambda')$, $\rho(\lambda')$, and $s_c(\lambda')$ are the wavelength of an incident light, the spectral intensity of a light source, the spectral reflectance of the surface, and the spectral sensitivity of the c channel ($c = R, G, B$) of the camera respectively. The geometric term of the diffuse reflection component g_d depends only on the lighting direction, while that of the specular reflection component g_s depends on both the lighting and viewing directions.

We assume that the object is illuminated by a narrow-band light source whose spectral intensity is approximately represented by using the Dirac delta function $\delta(\ )$ as

$$l(\lambda') = l\delta(\lambda' - \lambda). \qquad (3)$$

Substituting Eq.(3) into Eq.(2), we obtain

$$r_c = g_d l\rho(\lambda)s_c(\lambda) + g_s l s_c(\lambda), \qquad (4)$$

$$r = l(g_d\rho(\lambda) + g_s)\begin{pmatrix} s_R(\lambda) \\ s_G(\lambda) \\ s_B(\lambda) \end{pmatrix}. \qquad (5)$$

Therefore, the color of the reflective component, *i.e.* the reflective component normalized by its L_1 norm $\hat{r} = r/||r||_1$

under the narrow-band light source with the wavelength λ is described by the spectral sensitivity at the wavelength. This means that the color of the reflective component is the same as the light source color.

It is known that a pure fluorescent material absorbs light at a certain wavelength λ' and then emits light at a longer wavelength λ''. The fluorescent component is described as

$$f_c = g_f \int l(\lambda')a(\lambda')d\lambda' \int e(\lambda'')s_c(\lambda'')d\lambda'', \qquad (6)$$

where g_f, $a(\lambda')$, and $e(\lambda'')$ are the geometric term of the fluorescent component, the absorption and emission spectra of the fluorescent material.

Substituting Eq.(3) into Eq.(6), we obtain

$$f_c = g_f la(\lambda) \int e(\lambda'')s_c(\lambda'')d\lambda'', \qquad (7)$$

$$f = g_f la(\lambda)\begin{pmatrix} \int e(\lambda'')s_R(\lambda'')d\lambda'' \\ \int e(\lambda'')s_G(\lambda'')d\lambda'' \\ \int e(\lambda'')s_B(\lambda'')d\lambda'' \end{pmatrix}. \qquad (8)$$

Therefore, the color of the fluorescent component $\hat{f} = f/||f||_1$ under the narrow-band light source is independent of the wavelength λ of the light source. The light source wavelength affects only the scale of the fluorescent component through $a(\lambda)$.

3.2. Intersection method

We denote the pixel value observed under the n-th narrow-band light source ($n = 1, 2, 3, ..., N$) by i_n, and denote the corresponding reflective and fluorescent components by r_n and f_n respectively. Then, the pixel value i_n is represented by the convex combination of two unit vectors, *i.e.* the light source color $\hat{r}_n$ and the fluorescent color $\hat{f}_n$ as

$$i_n = r_n + f_n = \alpha_n \hat{r}_n + \beta_n \hat{f}, \qquad (9)$$

where α_n and β_n are the non-negative coefficients of the convex combination. As shown in the previous subsection, α_n, β_n, and $\hat{r}_n$ depend on the light source, but the fluorescent color $\hat{f}$ is independent of it.

Hereafter, we consider the RGB color space and the r-g chromaticity space defined by the spectral sensitivity of a camera, where $r = R/(R + G + B)$ and $g = G/(R + G + B)$ respectively. This is because the linearity in Eq.(9) is lost in nonlinear color spaces such as the CIE-L*a*b*. Our proposed method exploits the planar structure in the RGB color space and the linear structure in the r-g chromaticity space as described below.

Let us consider the case when $N = 2$. As shown in Figure 1 (a), for a certain pixel in the first image, Eq.(9) means that the fluorescent color $\hat{f}$ is on the plane spanned by the light source color $\hat{r}_1$ and the pixel color $\hat{i}_1 = i_1/||i_1||_1$.
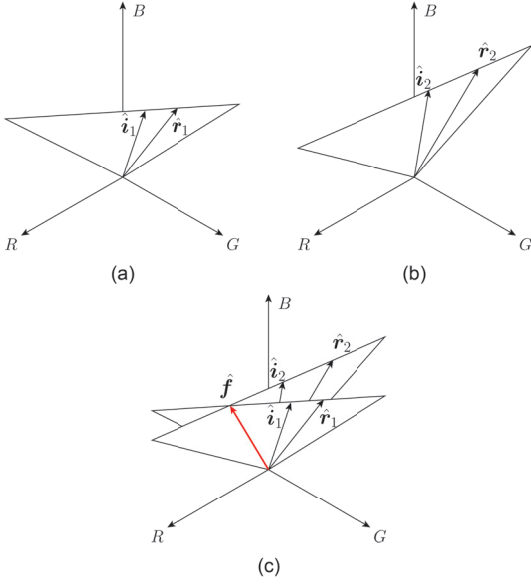
Figure 1. The illustration of the intersection method. The florescent color $\hat{f}$ is on (a) the plane spanned by the light source color $\hat{r}_1$ and the pixel color $\hat{i}_1$ and (b) the plane spanned by $\hat{r}_2$ and $\hat{i}_2$ at the same time. Therefore, the fluorescent color is given by (c) the intersection of those two planes.

Similarly, as shown in Figure 1(b), the fluorescent color $\hat{f}$ is on the plane spanned by the light source color $\hat{r}_2$ and the pixel color $\hat{i}_2$ in the second image at the same time. Therefore, the fluorescent color $\hat{f}$ is given by the intersection of those two planes as shown in Figure 1(c). Thus, we can separate the reflective components r_n and fluorescent components f_n per pixel from at least two images under the assumption that the light source colors $\hat{r}_n$ are known. Note that we can compute the coefficients of the convex combination α_n and β_n by using the least squares method with non-negativity constraints when the light source colors are known and the fluorescent color is given as the above.

In the general case when $N \geq 2$, the fluorescent color $\hat{f}$ is given by the intersection of the N planes. Specifically, the intersection method results in

$$
\begin{pmatrix} \vdots \\ (\hat{i}_n \times \hat{r}_n)^\top \\ \vdots \end{pmatrix} \hat{f} = \begin{pmatrix} \vdots \\ 0 \\ \vdots \end{pmatrix}, \tag{10}
$$

where $\times$ stands for the cross product. In practice, the fluorescent color $\hat{f}$ is computed by using the least squares method with non-negativity constraints.

Light source colors: Note that we can relax the assumption that the light source colors $\hat{r}_n$ are known. The pixel color $\hat{i}_n$ at a pure reflective pixel, where $f_n = 0$, is equal to the light source color $\hat{r}_n$ from Eq.(9). In addition, the pixel color at a reflective-fluorescent pixel is shifted towards red
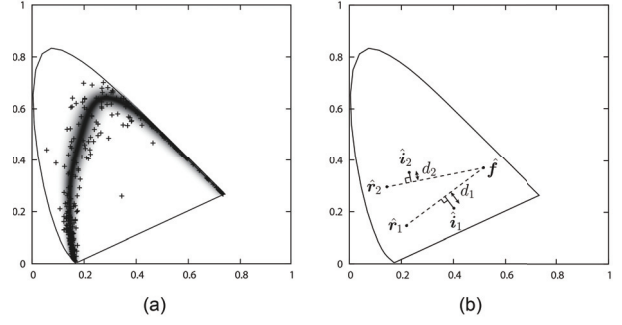

Figure 2. The prior and likelihood of MAP estimation. (a) The fluorescent colors computed from the actual emission spectra in the McNamara dataset [19]. The prior probability density of the fluorescent color is superimposed; darker has higher probability. (b) The sketch of the likelihood function. We assume that the distance d_n between the observed pixel color $\hat{i}_n$ and the line connecting from the light source color $\hat{r}_n$ to the fluorescent color $\hat{f}$ obeys the zero-mean Gaussian distribution.

due to the Stokes shift. Therefore, we can consider the most bluish pixel as a pure reflective pixel and consider its color as the light source color, if there is at least one pure reflective pixel in each image.

3.3. MAP estimation

The intersection method in Eq.(10) does not work well under the following two conditions. First, there is at most a single pair of $\hat{i}_n$ and $\hat{r}_n$ such that $\hat{i}_n \neq \hat{r}_n$, *i.e.* $\hat{i}_n \times \hat{r}_n \neq \mathbf{0}$. Second, there is no pair of $(\hat{i}_n \times \hat{r}_n)$ and $(\hat{i}_m \times \hat{r}_m)$ such that $(\hat{i}_n \times \hat{r}_n) \neq (\hat{i}_m \times \hat{r}_m)$. From the geometric point of view, the former means that there is at most a single plane and the latter means that the planes are parallel to each other in the RGB color space in Figure 1.

To cope with such limitations of the intersection method, our proposed method makes use of the prior knowledge with respect to fluorescent colors. In Figure 2 (a), we plot the fluorescent colors computed from the actual emission spectra in the McNamara dataset [19] in the chromaticity space[2]. We can see that the distribution of fluorescent colors has arch-like structure, in particular reddish colors distribute near the spectrum locus, *i.e.* the locus of the monochromatic (single-wavelength) color. This is because the emission spectra are relatively narrow-band.

Accordingly, we formulate the estimation of the fluorescent color via MAP estimation as

$$
\max_{\hat{f}} \prod_{n=1}^{N} P(\hat{i}_n | \hat{f}; \hat{r}_n) P(\hat{f}). \tag{11}
$$

---

[2]Here, we assume the x-y chromaticity space defined by the CIE-XYZ for display purpose, where $x = X/(X+Y+Z)$ and $y = Y/(X+Y+Z)$ respectively. Our proposed method assumes that the spectral sensitivity of a camera is known and considers the prior probability distribution of fluorescent colors in the r-g chromaticity space defined by the camera.

Here, $P(\hat{\boldsymbol{i}}_n|\hat{\boldsymbol{f}};\hat{\boldsymbol{r}}_n)$ is the likelihood function, *i.e.* the probability density that the pixel color $\hat{\boldsymbol{i}}_n$ is observed when the fluorescent color $\hat{\boldsymbol{f}}$ is given and the light source color $\hat{\boldsymbol{r}}_n$ is known, and $P(\hat{\boldsymbol{f}})$ is the prior probability density of the fluorescent color $\hat{\boldsymbol{f}}$. Taking the natural log of the above objective function, we obtain

$$\max_{\hat{\boldsymbol{f}}}\left[\sum_{n=1}^{N}\log P(\hat{\boldsymbol{i}}_n|\hat{\boldsymbol{f}};\hat{\boldsymbol{r}}_n) + \log P(\hat{\boldsymbol{f}})\right]. \quad (12)$$

It is clear from Eq.(9) that the light source color $\hat{\boldsymbol{r}}_n$, the fluorescent color $\hat{\boldsymbol{f}}$, and the pixel color $\hat{\boldsymbol{i}}_n$ are on a single line in the r-g chromaticity space[3]. In practice, however, the observed pixel color is not on the line connecting from the light source color $\hat{\boldsymbol{r}}_n$ to the fluorescent color $\hat{\boldsymbol{f}}$ due to the noise in the observed pixel value. We assume that the distance d_n between the observed pixel color $\hat{\boldsymbol{i}}_n$ and the line in the chromaticity space (see Figure 2 (b)) obeys the zero-mean Gaussian distribution[4] as

$$P(\hat{\boldsymbol{i}}_n|\hat{\boldsymbol{f}};\hat{\boldsymbol{r}}_n) = \frac{1}{2\pi\sigma^2}\exp\left(-\frac{d_n^2}{2\sigma^2}\right). \quad (13)$$

Then, the first term in Eq.(12) results in

$$-\frac{1}{2\sigma^2}\sum_{n=1}^{N}d_n^2, \quad (14)$$

where we omit constant terms independent of $\hat{\boldsymbol{f}}$.

Figure 2 (a) shows that the McNamara dataset has a bias; the number of fluorescent materials with bluish emission spectra is larger than the number of those with greenish and reddish spectra. To prevent the bias from propagating to the result of the MAP estimation, we fit a smoothing spline curve to the distribution of fluorescent colors in Figure 2 (a)[5], and approximate the prior probability density of the fluorescent color $P(\hat{\boldsymbol{f}})$ by using the Gaussian distributions whose centers are at the points on the spline curve. The variances of the Gaussian distributions are computed around the points on the spline curve. The computed prior probability density $P(\hat{\boldsymbol{f}})$ is superimposed in Figure 2 (a); darker has higher probability

Thus, our proposed method based on the MAP estimation results in

$$\min_{\hat{\boldsymbol{f}}}\left[\frac{1}{2}\sum_{n=1}^{N}d_n^2 - \sigma^2\log P(\hat{\boldsymbol{f}})\right]. \quad (15)$$

Since the above optimization is non-linear, we find the optimal fluorescent color via coarse-to-fine search in the chromaticity space. Note that the fluorescent color is more reddish than the pixel color due to the Stokes shift and because the pixel color is represented by a convex combination of the light source color and the fluorescent color. Thus, we constrain the search area to $\hat{f}_r + \hat{f}_g \geq \hat{i}_r + \hat{i}_g$ within the spectrum locus.

Single-image method: Note that our proposed method based on the MAP estimation enables us to separate reflective and fluorescent components even from a single image. Intuitively, a single image constrains the fluorescent color up to the neighborhood of the line connecting from the light source color towards the pixel color from Eq.(9). Then, the prior knowledge further constrains the fluorescent color up to the neighborhood of the fitted smoothing spline curve. Therefore, the fluorescent color estimated from a single image is located near their intersection.

4. Experiments

4.1. Synthetic images

We compared the performances of our proposed methods with that of the closely related state-of-the-art method [26] by using synthetic images. Specifically, we compared the following four methods.

- **Zhang and Sato [26] (ICA)** assumes a narrow-band camera and is based on the channel-wise linear model. The ordering ambiguity in ICA is resolved by using known light source colors in our experiments[6].

- **Intersection method (IS)** assumes narrow-band illumination and is based on the pixel-wise linear model. As described in Subsection 3.2, the fluorescent color is given by the intersection of the two planes.

- **MAP estimation (MAP)** extends the intersection method by taking the prior knowledge with respect to fluorescent colors into consideration as described in Subsection 3.3. Multiple images are used as input.

- **MAP estimation from a single image (MAP single)** is the same as the above MAP estimation in its formulation, but a single image is used as input.

We synthesized the images of spheres with different spectral properties taken by cameras with different spectral sensitivities under light sources with different peak wavelengths and widths. We used the spectral reflectances of matte Munsell color chips [22], the absorption and emission spectra in the McNamara dataset [19], and the dataset of camera spectral sensitivity [14] for synthesizing realistic images. We assumed that the spectral intensities of light

---

[3]For the sake of simplicity, we denote an unit vector in the RGB color space and its projection to the r-g chromaticity space by the same symbol.

[4]Although σ could depend on the pixel value $\boldsymbol{i}$, we fixed it to 0.01 in all of our experiments.

[5]We considered a fluorescent color of $(0.34, 0.26)$ as an outlier and removed it from the computation.

[6]The reflective and fluorescent components estimated by using ICA can be negative. We clipped them to zeros in our experiments.

Table 1. The quantitative comparison using the first object under varying σ_w and σ_n. The numerical value in each cell stands for the RMS error of four result images.

$\sigma_n \backslash \sigma_w$	ICA				IS				MAP				MAP single			
	5	10	15	20	5	10	15	20	5	10	15	20	5	10	15	20
0	39.3	38.5	38.3	38.9	0.8	0.8	1.0	1.2	0.9	0.9	1.0	1.4	6.4	4.9	4.1	5.2
1	38.9	38.2	38.5	38.8	2.6	2.6	2.6	2.8	2.5	2.4	2.3	2.4	7.9	6.3	5.3	8.1
2	39.1	38.4	38.3	38.6	5.1	5.1	5.1	5.2	4.7	4.7	4.5	4.4	10.3	8.7	7.6	8.9
4	38.8	38.4	38.4	38.7	10.4	10.2	10.2	10.1	10.0	9.7	9.5	8.9	15.3	13.5	12.3	12.0

Table 2. The quantitative comparison using the second object under varying σ_w and σ_n.

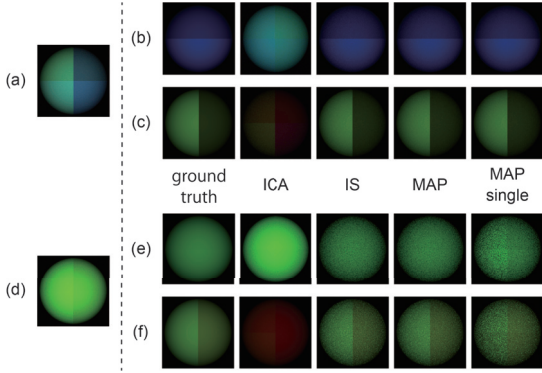| $\sigma_n \backslash \sigma_w$	ICA				IS				MAP				MAP single			
	5	10	15	20	5	10	15	20	5	10	15	20	5	10	15	20
0	17.7	18.0	18.6	19.4	2.3	2.4	2.5	2.7	4.3	4.3	4.4	4.5	4.4	4.5	4.6	4.8
1	18.3	17.9	18.6	19.4	7.4	7.3	7.1	7.0	4.6	4.7	4.8	4.9	4.6	4.7	4.9	5.1
2	17.7	18.5	18.6	19.5	13.0	12.7	12.4	12.3	6.9	6.8	7.0	7.1	5.6	5.6	5.9	6.2
4	17.9	18.2	19.1	20.0	19.6	19.2	19.0	19.1	10.7	10.8	11.0	11.2	9.1	9.3	9.4	9.9

Figure 3. The qualitative comparison using the first object. (a) (d) are the input images. (b) (e) and (c) (f) are the corresponding reflective and fluorescent images: the ground truth and the results using ICA, IS, MAP, and MAP single from left to right.

Figure 4. The qualitative comparison using the second object.

sources obey the Gaussian distributions with the standard deviation σ_w. In order to evaluate the robustness of those methods against noises, we artificially added the zero-mean Gaussian noise with the standard deviation σ_n to each pixel.

Figure 3 shows the qualitative comparison using the first object. (a) (d) are the input images; the peak wavelengths of light sources are 475 nm and 525 nm respectively and the camera is Nikon D300s. (b) (e) and (c) (f) are the corresponding reflective and fluorescent images: the ground truth and the results using ICA, IS, MAP, and MAP single from left to right. Here, σ_w is 10 nm and σ_n is 2 for 8-bit images. Table 1 shows the quantitative comparison using the first object under varying σ_w and σ_n. The numerical value in each cell stands for the root mean square (RMS) error of four result images: the reflective component and the fluorescent component for the first input image and those for the second input image. Figure 4 and Table 2 show the results using the second object. The peak wavelengths of light sources are 425 nm and 475 nm respectively and the camera
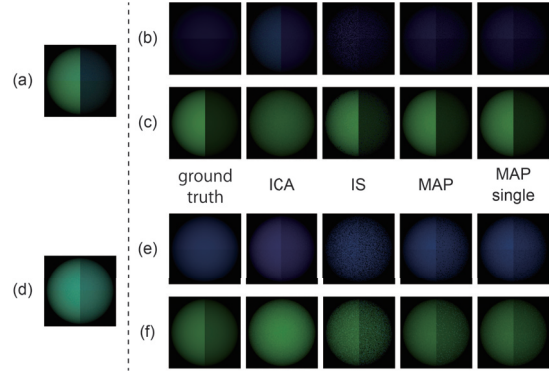
is Canon 5D Mark II.

ICA vs. IS, MAP, and MAP single: Figure 3, Figure 4, Table 1, and Table 2 show both qualitatively and quantitatively that our proposed methods, *i.e.* IS, MAP, and MAP single work better than the state-of-the art method [26] (ICA) for images under narrow-band illumination. In addition, they are robust when the widths of spectral intensities σ_w increase from 5 nm to 20 nm. Note that the full width at half maximum (FWHM) is about $2.35 \times \sigma_w$.

IS vs. MAP: Figure 3 and Table 1 show that both of IS and MAP work well, but Figure 4 and Table 2 show that MAP works better than IS in particular when σ_n increases. In the former case, the light source colors of the input images[7] are different. Therefore, as shown in Figure 1 (c), we can obtain two planes such that $(\hat{\boldsymbol{i}}_1 \times \hat{\boldsymbol{r}}_1) \neq (\hat{\boldsymbol{i}}_2 \times \hat{\boldsymbol{r}}_2)$, and then IS itself works well. On the other hand, in the latter case, the light source colors of the input images are similar to each other. Therefore, the two planes in the RGB color space are also similar, and then IS is not stable and the prior knowledge with respect to fluorescent colors is effective.

MAP vs. MAP single: Figure 4 and Table 2 show that

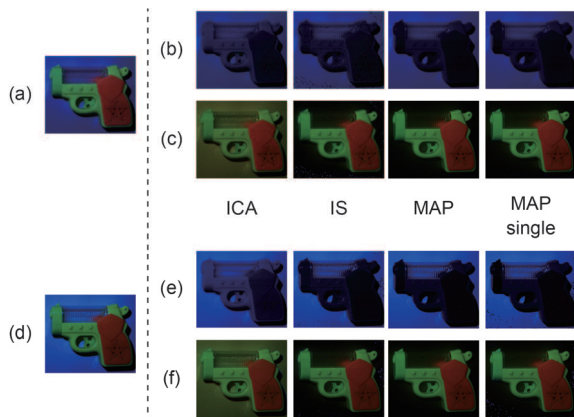[7]See the ground truth of the reflective images in (b) and (e).

Figure 5. The qualitative comparison using the real images of a water pistol under the first and the second light source colors. (a) (d) are the input images. (b) (e) and (c) (f) are the corresponding reflective and fluorescent images: the results using ICA, IS, MAP, and MAP single from left to right.
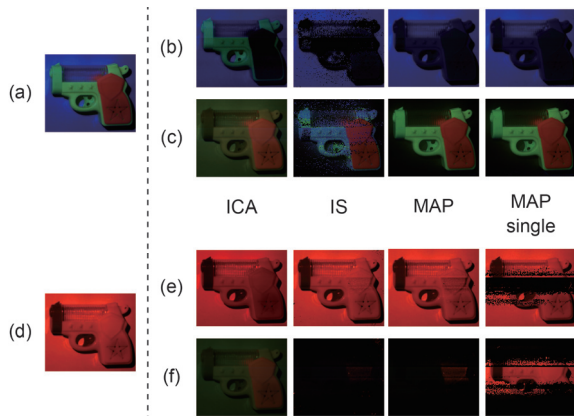

Figure 6. The qualitative comparison using the real images of a water pistol under the first and the fourth light source colors.
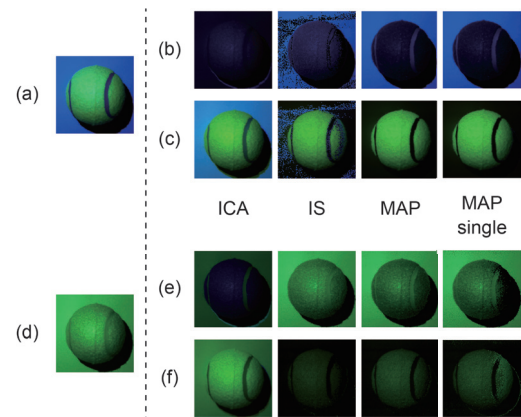

Figure 7. The qualitative comparison using the real images of a tennis ball under the second and the third light source colors.

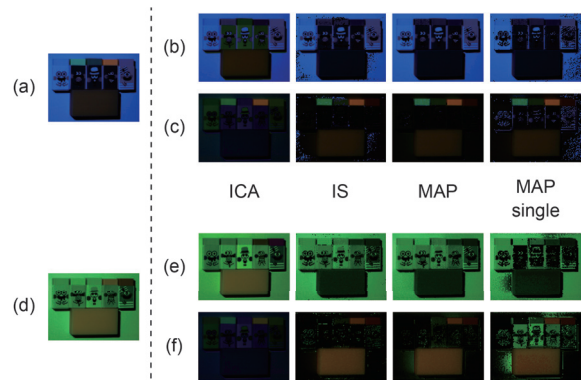Figure 8. The qualitative comparison using the real images of erasers under the second and the third light source colors.

the performance of MAP single is almost the same as that of MAP using two input images, when the light source color is different from the fluorescent color. In the case where they are similar (Figure 3 and Table 1), the single image method has its limits. The separation is not satisfying, because the linear constraint in Eq.(9) could be sensitive to noises.

As described in Section 3, we have two different clues for estimating fluorescent colors; one is a single linear constraint in Eq.(9) per input image, and the other is the constraint due to the prior knowledge with respect to fluorescent colors. Specifically, for two input images, IS has two linear constraints, and MAP has two linear constraints and the constraint due to the prior. MAP single has one linear constraint and the constraint due to the prior for a single input image. The experimental results show that our proposed methods work well when at least two independent

constraints are effective.

4.2. Real images

We compared the performances of our proposed methods (IS, MAP, and MAP single) with that of the closely related state-of-the-art method (ICA) [26] by using real images. The target objects are a water pistol, a tennis ball, and erasers. The images of those objects were captured by using a Point Grey Chameleon camera under four different LEDs whose peak wavelengths are 405, 460, 520, and 635 nm respectively and FWHMs are from 12 to 36 nm.

Figure 5 shows the qualitative comparison using the real images of the water pistol under the first (405 nm) and the second (460 nm) LEDs. (a) (d) are the input images. (b) (e) and (c) (f) are the corresponding reflective and fluorescent images: the results using ICA, IS, MAP, and MAP single from left to right. Figure 6, Figure 7, and Figure 8 show the qualitative comparisons using the real images of the water pistol, the tennis ball, and the erasers respectively. We used the first and the fourth (635 nm) LEDs in Figure 6, and the
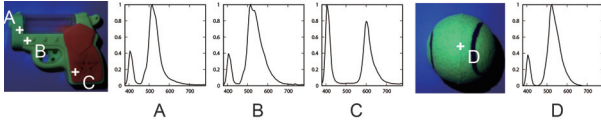
Figure 9. The spectral radiances observed at the points A, B, and C on the water pistol and the point D on the tennis ball under the first light source.

Table 3. The quantitative comparison using real images: the dot products between the ground truth and estimated fluorescent colors.

	A	B	C	D
ICA	0.919	0.931	0.992	0.960
IS	0.982	0.989	0.996	0.996
MAP	0.983	0.991	0.999	0.998
MAP single	0.983	0.992	0.999	0.998

second and the third (520 nm) LEDs in Figure 7 and Figure 8.

ICA vs. IS, MAP, and MAP single: We can see that our proposed methods (IS, MAP, and MAP single) work better than ICA. In particular, the colors of the reflective components estimated by ICA are different from the light source colors in Figure 6 (b) and Figure 8 (b) (e). In addition, the fluorescence of the orange eraser disappears from the fluorescent components estimated by ICA in Figure 8 (c) (f).

IS vs. MAP: We can see that MAP is more robust than IS. In particular, the effectiveness of MAP, *i.e.* taking account of the prior knowledge with respect to fluorescent colors is clear when one of the input images has no clue about fluorescent colors as shown in Figure 6 (b) (c) and (e) (f). Figure 7 also shows that MAP works better than IS.

MAP vs. MAP single: We can see that MAP single works as well as MAP as shown in Figure 5 (b) (c) and (e) (f), Figure 6 (b) (c), Figure 7 (b) (c), and Figure 8 (b) (c). On the other hand, when the light source colors are similar to the fluorescent colors, MAP single is not robust as shown in Figure 7 (e) (f) and Figure 8 (e) (f), and does not work well as shown in Figure 6 (e) (f).

To confirm the effectiveness of our proposed methods quantitatively, we conducted numerical comparison using a hyperspectral camera. Specifically, as shown in Figure 9, we measured the spectral radiances under the first light source (405 nm) at the points A, B, and C on the water pistol and at the point D on the tennis ball. Since the emission spectra are separated from the reflection spectra, we can compute the fluorescent colors there by using the spectral sensitivity of the color camera, and consider them as their ground truths. Table 3 shows the dot products between the ground truth and estimated colors in Figure 5 (c) and Figure 7 (c). Here, both colors are represented by unit 3D vectors, and then the dot product is 1 if the colors are the
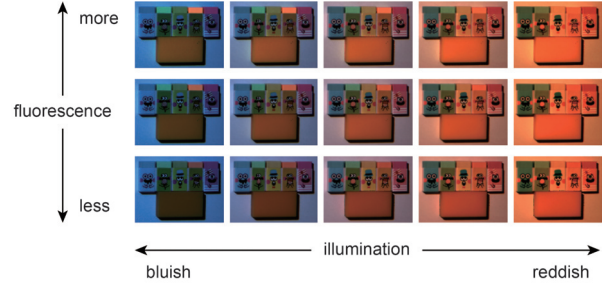

Figure 10. The application of our reflective-fluorescent separation to image-based material editing and relighting.

same. These results show quantitatively that our proposed methods (IS, MAP, and MAP single) work better than ICA.

4.3. Applications

As a direct application of reflective-fluorescent separation, we conducted image-based material editing and relighting. Specifically, we captured three images of the erasers under B (the first), G (the third), and R (the fourth) light sources, and separated the reflective and fluorescent components of those images by using our proposed method (MAP). Then, we synthesized various images by linearly combining those 6 images with different weights. In Figure 10, their average is shown at the center (the second row and the third column), and the fluorescent components are increased/decreased at the upper/lower images. Similarly, we change the light source colors from bluish (left) to reddish (right). We can see that our method is effective for photorealistic image-based material editing and relighting.

5. Conclusion and Future Work

In this paper, we showed that the fluorescent color per pixel can be estimated from at least two images under different light source colors. Furthermore, exploiting the known space of potential fluorescent colors, we obtain more robust MAP estimates even from a single input image under narrow-band illumination. Through a number of experiments using both synthetic and real images, we confirmed qualitatively and quantitatively that our proposed method works better than the closely related state-of-the-art method. In addition, we demonstrated that our method is effective for image-based material editing and relighting. Incorporating the spectral-spatial correlation into our pixel-wise approach is one of the future directions of this study.

Acknowledgments

References

[1] B. Ajdin, M. Finckh, C. Fuchs, J. Hanika, and H. Lensch. Compressive higher-order sparse and low-rank acquisition with a hyperspectral light stage. Technical report, Eberhard Karls Universität Tübingen, 2012. WSI-2012-01. 1

[2] K. Barnard. Color constancy with fluorescent surfaces. In *Proc. CIC1999*, pages 257–261, 1999. 1

[3] R. Donaldson. Spectrophotometry of fluorescent pigments. *British Journal of Applied Physics*, 5(6):210–214, 1954. 2

[4] H. Farid and E. Adelson. Separating reflections and lighting using independent components analysis. In *Proc. IEEE CVPR1999*, pages I–262–267, 1999. 2

[5] Y. Fu, A. Lam, I. Sato, T. Okabe, and Y. Sato. Reflectance and fluorescence spectral recovery via actively lit RGB images. *IEEE Trans. PAMI*, 38(7):1313–1326, 2016. 2

[6] Y. Fu, A. Lam, I. Sato, T. Okabe, and Y. Sato. Separating reflective and fluorescent components using high frequency illumination in the spectral domain. *IEEE Trans. PAMI*, 38(5):965–978, 2016. 2

[7] A. Glassner. A model for fluorescence and phosphorescence. In *Proc. the 5th Eurographics Workshop on Rendering*, pages 57–68, 1994. 2

[8] J. Gu and C. Liu. Discriminative illumination: per-pixel classification of raw materials based on optimal projections of spectral BRDF. In *Proc. IEEE CVPR2012*, pages 797–804, 2012. 1

[9] S. Han, Y. Matsushita, I. Sato, T. Okabe, and Y. Sato. Camera spectral sensitivity estimation from a single image under unknown illumination by using fluorescence. In *Proc. IEEE CVPR2012*, pages 805–812, 2012. 2

[10] M. Hullin, M. Fuchs, I. Ihrke, H.-P. Seidel, and H. Lensch. Fluorescent immersion range scanning. In *Proc. ACM SIGGRAPH2008*, 2008. Article No.87. 2

[11] M. Hullin, J. Hanika, B. Ajdin, H.-P. Seidel, J. Kautz, and H. Lensch. Acquisition and analysis of bispectral bidirectional reflectance and reradiation distribution functions. In *Proc. ACM SIGGRAPH2010*, 2010. Article No.97. 2

[12] A. Hyvärinen and E. Oja. Independent component analysis: algorithms and applications. *Neural Networks*, 13(4–5):411–430, 2000. 1

[13] D. Jameson. *Introduction to fluorescence*. CRC Press, 2014. 2

[14] J. Jiang, D. Liu, J. Gu, and S. Süsstrunk. What is the space of spectral sensitivity functions for digital color cameras? In *Proc. IEEE WACV2013*, pages 168–179, 2013. 5

[15] M. Kitahara, T. Okabe, C. Fuchs, and H. Lensch. Simultaneous estimation of spectral reflectance and normal from a small number of images. In *Proc. VISAPP2015*, pages 303–313, 2015. 1

[16] C. LeGendre, X. Yu, D. Liu, J. Busch, A. Jones, S. Pattanaik, and P. Debevec. Practical multispectral lighting reproduction. In *Proc. ACM SIGGRAPH2016*, 2016. Article No.32. 1

[17] C. Liu, G. Yang, and J. Gu. Learning discriminative illumination and filters for raw material classification with optimal projections of bidirectional texture functions. In *Proc. IEEE CVPR2013*, pages 1430–1437, 2013. 1

[18] S. Marschner, S. Westin, E. Lafortune, and K. Torrance. Image-based bidirectional reflectance distribution function measurement. *Applied Optics*, 39(16):2592–2600, 2000. 2

[19] G. McNamara, A. Gupta, J. Reynaert, T. Coates, and C. Boswell. Spectral imaging microscopy web sites and data. *Cytometry Part A*, 69A(8):863–871, 2006. 3, 4, 5

[20] S. Nayar, G. Krishnan, M. Grossberg, and R. Raskar. Fast separation of direct and global components of a scene using high frequency illumination. In *Proc. ACM SIGGRAPH 2006*, pages 935–944, 2006. 2

[21] J.-I. Park, M.-H. Lee, M. Grossberg, and S. Nayar. Multispectral imaging using multiplexed illumination. In *Proc. IEEE ICCV2007*, pages 1–8, 2007. 1

[22] J. Parkkinen, J. Hallikainen, and T. Jaaskelainen. Characteristic spectra of munsell colors. *JOSA A*, 6(2):318–322, 1989. 2, 5

[23] I. Sato, T. Okabe, and Y. Sato. Bispectral photometric stereo based on fluorescence. In *Proc. IEEE CVPR2012*, pages 270–277, 2012. 2

[24] T. Treibitz, Z. Murez, G. Mitchell, and D. Kriegman. Shape from fluorescence. In *Proc. ECCV2012*, pages 292–306, 2012. 2

[25] A. Wilkie, A. Weidlich, C. Larboulette, and W. Purgathofer. A reflectance model for diffuse fluorescent surfaces. In *Proc. GRAPHITE2006*, pages 321–331, 2006. 2

[26] C. Zhang and I. Sato. Image-based separation of reflective and fluorescent components using illumination variant and invariant color. *IEEE Trans. PAMI*, 35(12):2866–2877, 2013. 1, 2, 5, 6, 7